J Therm Anal Calorim (2016) 126:1463–1468
DOI 10.1007/s10973-016-5716-z

Investigation of the enthalpy/entropy variation and structure of Ni–Mn–Sn (Co, In) melt-spun alloys

T. Bachaga[1,2] · H. Rekik[1] · M. Krifa[1] · J. J. Suñol[2] · M. Khitouni[1]

Received: 7 February 2016 / Accepted: 15 July 2016 / Published online: 25 July 2016

Abstract The effect of In and Co additions on the structure and thermal properties of melt-spun process Ni–Mn–Sn alloys has experimentally investigated at a solidification rate of $\sim$48 m s^{-1}. The present study reports on the analysis of the microstructure, martensitic transformation of $Ni_{50}Mn_{42.5}Sn_{7.5}$, $Ni_{50}Mn_{37.5}Sn_{7.5}Co_5$ and $Ni_{50}Mn_{37}Sn_{6.5}In_{6.5}$. Heusler alloys produced by melt spinning. The crystal structures of the fabricated alloys were determined by means of X-ray diffraction. While the as-spun alloy $Ni_{50}Mn_{42.5}Sn_{7.5}$ displayed a single-phase (14M monoclinic martensite) structure at room temperature, the as-spun $Ni_{50}Mn_{37.5}Sn_{7.5}Co_5$ displayed a main martensitic phase of a four-layered orthorhombic (4O) structure and the as-spun $Ni_{50}Mn_{37}Sn_{6.5}In_{6.5}$ displayed a single-phase cubic Heusler $L2_1$. The characteristic transformation temperatures and the thermodynamic parameters of the samples were determined by differential scanning calorimetry measurements. This study investigated the effect of the substitution of Co by Mn in $Ni_{50}Mn_{42.5-x}Sn_{7.5}Co_x$. The martensitic transformation temperatures, enthalpy and entropy changes were found to increase progressively with doping Co content and the effect of the substitution of In by Mn. The martensitic transformation temperatures, enthalpy and entropy changes were found to decrease progressively with doping In.

Keywords Shape memory alloy · Melt-spun process · Martensitic transformation · X-ray diffraction

✉ T. Bachaga
bachagatarak@yahoo.fr

[1] Laboratory of Inorganic Chemistry, UR 11ES73, University of Sfax, Soukra Road km 3,5, B. P. 1171, 3018 Sfax, Tunisia

[2] Dep. de Física, Universitat de Girona, Campus de Montilivi, 17071 Girona, Spain

Introduction

Heusler alloys of the general formula Ni–Mn–X (X = Sb, In, Sn) have attracted considerable attention due to their diverse multifunctional properties associated with the first-order solid-state martensitic transformation (MT) [1]. In these systems, MT occurs between the ferromagnetic austenite phase, with the cubic $L2_1$ structure, and a martensite phase with clearly lower magnetic susceptibility and with various structural configurations. The latter depend on composition and fabrication methods and include 10M, 14M, 4O or $L1_0$ structures [2]. Recent research works have proven that melt-spinning technique could effectively generate highly textured homogeneous polycrystalline ribbons [3, 4] and substantially enhance magnetic properties [5]. It is interesting that the martensitic transformation of the Heusler Ni–Mn–X ribbons always occurs at a lower temperature as compared with their bulk alloy. For instance, Santos et al. [6] have found that the martensitic transformation of $Ni_{50}Mn_{37}Sn_{13}$ ribbons occurs at about 212 K, while Krenke et al. [7] and Wang et al. [8] have reported it to take place in the vicinity of 300 K in the bulk alloy. "Metamagnetic shape memory alloys," which were firstly named by Kainuma et al. [9], have attracted much attention as multifunctional materials thanks to their large magnetic-field-induced shape recovery [9–11], magnetocaloric effect [12–14] and magnetoresistance [15, 16]. As one of the most important branches of metamagnetic shape memory alloys, NiCoMnSn has been investigated by many researchers, especially its martensitic and magnetic transition behavior, microstructure, as well as magnetic property [16–23]. All these interesting physical properties are closely linked to the magnetization discrepancy (ΔM) between the austenite and the martensite [24]. It is found that Co doping strongly affects the ΔM in Heusler Ni–Mn-based materials. Liu et al. [25] have observed that the

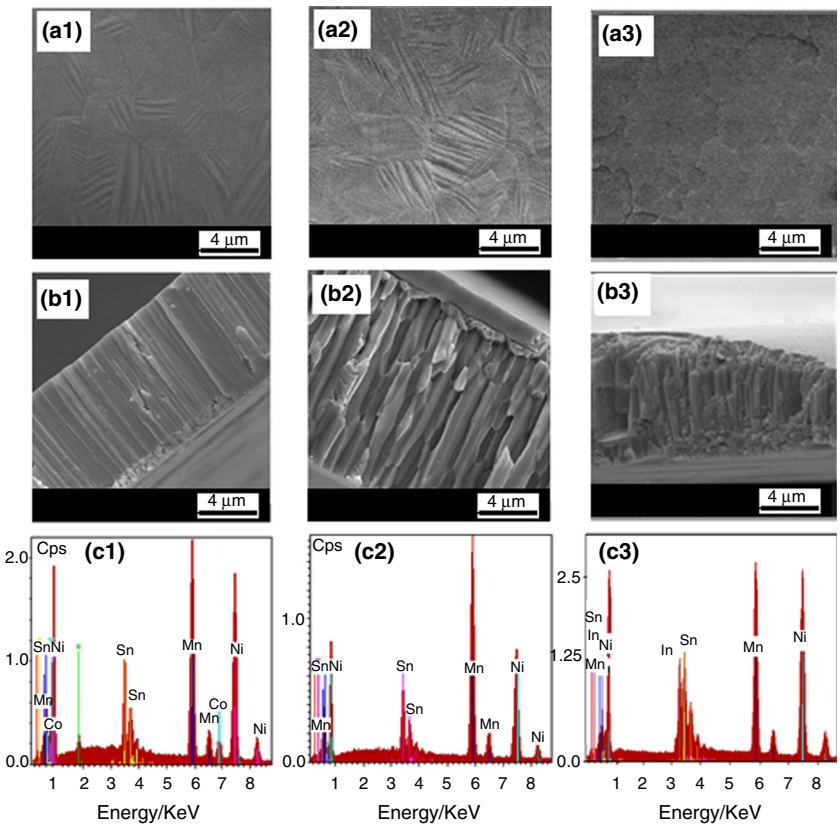

Fig. 1 X-ray diffraction pattern at room temperature for A1, A2 and A3 samples, respectively

ΔM across the martensitic transformation increases dramatically from 0.03 to 50 emu g^{-1} in $Ni_{45}Co_5Mn_{37}In_{13}$ in contrast to the $Ni_{49}Co_1Mn_{37}In_{13}$.

In this study, we consider three alloys in the Ni–Mn–Sn system (by modifying the chemical composition) in order to develop materials with a martensite–austenite transformation temperature range above, near or below room temperature. We outline the microstructural and phase transition characteristics of melt-spun ribbons with starting selected compositions $Ni_{50}Mn_{42.5}Sn_{7.5}$, $Ni_{50}Mn_{37.5}Sn_{7.5}Co_5$ and $Ni_{50}Mn_{37}Sn_{6.5}In_{6.5}$.

Experimental

As-cast ingots with a nominal composition of $Ni_{50}Mn_{37.5}Sn_{7.5}Co_5$ (named A1), $Ni_{50}Mn_{42.5}Sn_{7.5}$ (named A2) and $Ni_{50}Mn_{37}Sn_{6.5}In_{6.5}$ (named A3) were prepared by arc-melting technique in argon atmosphere from high-purity (99.99 %) elemental metals, using Bühler MAM-1 compact arc melter. Ingots were melted four times to ensure a good starting homogeneity. The samples were induction-melted in quartz crucibles with a circular nozzle of 0.6 mm and ejected applying an argon overpressure on the polished surface of copper wheel rotating at a linear speed of 48 m s^{-1}. The obtained as-quenched ribbons were flakes of 1.2–2.0 mm in width and 4–12 mm in length. Microstructure and elemental compositions were examined by using a scanning electron microscope (SEM) equipped with an energy-dispersive X-ray spectroscopy (EDX) microanalysis system. The process was carried out in argon environment. X-ray diffraction (XRD) analyses were performed at room temperature with a Siemens D500 X-ray powder diffractometer using Cu-K_α radiation (K_α-Cu = 0.15406 nm). The structures of samples are refined by using Maud Program [26] and Jana software [27]. The austenite–martensite structural transformation was checked by calorimetry. The cyclic experiments (heating–cooling) were recorded at 10 °C min^{-1} under argon atmosphere. DSC scans above room temperature were performed in the DSC high-temperature DSC modulus of the Setaram Setsys system, and the DSC scan below room temperature was performed in the DSC 30 device of Mettler–Toledo working with a liquid nitrogen cooling system. The DSC measurements were carried out to examine the characteristic temperatures of MT, and the phase-transition activation energy was calculated on the basis of the DSC measurements.

Results and discussion

The alloys studied: $Ni_{50}Mn_{37.5}Sn_{7.5}Co_5$, $Ni_{50}Mn_{42.5}Sn_{7.5}$ and $Ni_{50}Mn_{37}Sn_{6.5}In_{6.5}$ are named by A1, A2 and A3, respectively. The typical SEM images of the wheel surfaces of A1, A2 and A3 ribbons are presented in Fig. 1a_1–a_3, respectively. The wheel surfaces of the A1 and A2 ribbons clearly present the lamellar microstructure of the martensite structure (Fig. 1a_1, a_2). These ribbons are mechanically fragile and brittle and cleave easily along the perpendicular direction to the ribbon plane, while the wheel surface of the A3 ribbons is characterized by a granular microstructure of the austenite structure (Fig. 1a_3). The cross sections for A1, A2 and A3 alloys normal to ribbon planes can be observed in Fig. 1b_1–b_3, respectively. They demonstrate that the samples were fully crystalline and their fracture surfaces revealed a fast crystallization and growth kinetics of the alloy. It also showed a collinear granular columnar-type microstructure (Fig. 1b_1–b_3). The A1, A2 and A3 ribbon thickness was around 10, 15 and 8 μm, respectively. The thin layer of small equiaxed grains crystallized through the whole ribbon thickness, with the longest axis being aligned perpendicular to the ribbon plane. The obtained results of EDX microanalysis of chemical composition examined by scanning electron microscope (SEM) show conformity with assumption of the chemical composition of the studied as-spun ribbons (Fig. 1c_1–c_3). The composition analysis was found to be in good agreement with the nominal compositions of the as-spun ribbons (50.3 at% Ni-37.4 at% Mn-7.4 at% Sn-4.9 at% Co), (50.4 at% Ni-42.2 at% Mn-7.4 at% Sn) and (50.4 at% Ni-36.7 at% Mn-6.3 at% Sn-6.6 at% In). The EDX analysis of the as-spun ribbons is shown in Fig. 1c_1–c_3. The results confirm the presence of the mixed metallic elements.

To determine the thermal analysis conditions, the knowledge of crystal structure at room temperature is important. If the cubic phase is detected, the martensite-austenite transition must be below room temperature. Yet, the same transition is revealed by heating the alloy from the room temperature if the revealed phase is orthorhombic, monoclinic or tetragonal. Figure 2a_1–a_3 shows the XRD patterns of A1, A2 and A3 ribbons analyzed at room temperature. The fitting parameter Rp values are 0.092, 0.0831 and 0.0921 for samples A1, A2 and A3, respectively. As shown in Fig. 2a_1, the XRD patterns of A1 ribbons illustrate a main martensitic phase of a four-layered orthorhombic (4O) structure with lattice parameters $a = 0.8922(1)$, $b = 0.5892(2)$ and $c = 0.4281(1)$ nm. Miller indexes were assigned with the aid of indexing programs as Treor and Dicvol. Figure 2a_2 presents the XRD patterns of A2 ribbons obtained at room temperature. The diffractogram demonstrates a martensitic phase of monoclinic 14M structure with lattice parameter: $a = 0.4301(3)$, $b = 0.5610(4)$, $c = 2.996(1)$ nm: $\beta = 93.77°$. The inset of Fig. 2a_2 corresponds to the range of $40° \leq 2\theta \leq 50°$. This may indicate that the temperature of the martensitic transformation (M_T) is in the vicinity of room temperature. However, for A3 ribbons, the XRD patterns indicate that the crystalline austenite phase was the highly ordered cubic Heusler $L2_1$ with lattice parameter $a = 0.5960$ (1) nm (Fig. 2a_3).

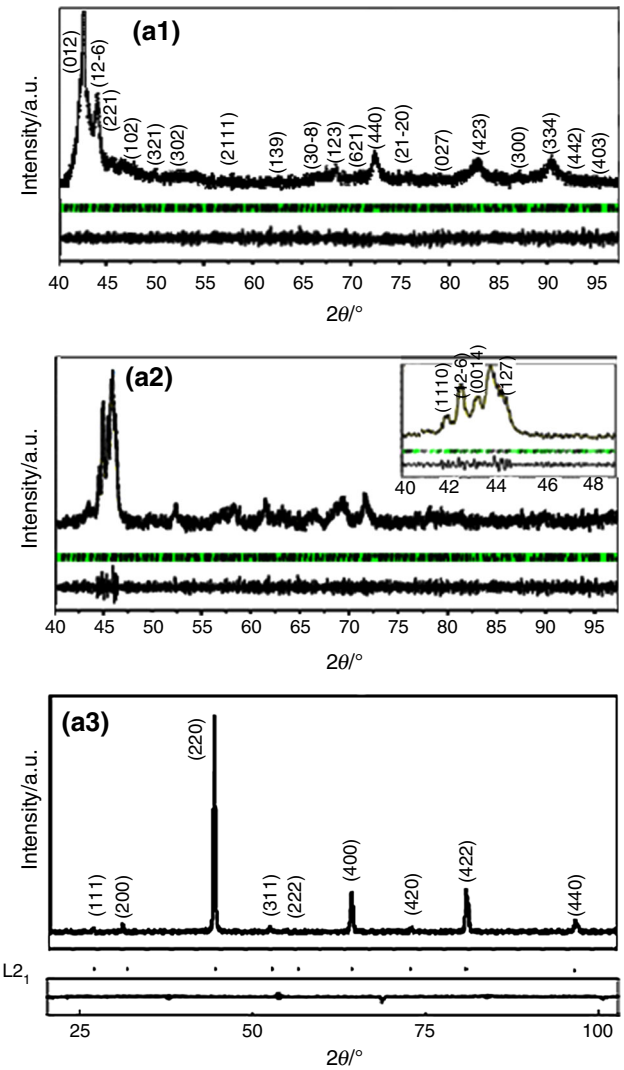

Fig. 2 Typical SEM micrographs of the different regions:(a1-a3) wheel surfaces, (b1-b3) fractured cross sections and (c1-c3) EDS analyses of A1, A2 and A3 alloys, respectively

On the basis of the XRD results, it is clear that the DSC scans of A1 and A2 ribbons should be performed by heating from room temperature in order to detect the martensite-austenite transition while the DSC scan of A3 alloy could be performed by cooling from room temperature. The corresponding DSC results are given in Fig. 3a_1–a_3. The characteristic transformation temperatures (martensite start and finish and austenite start and

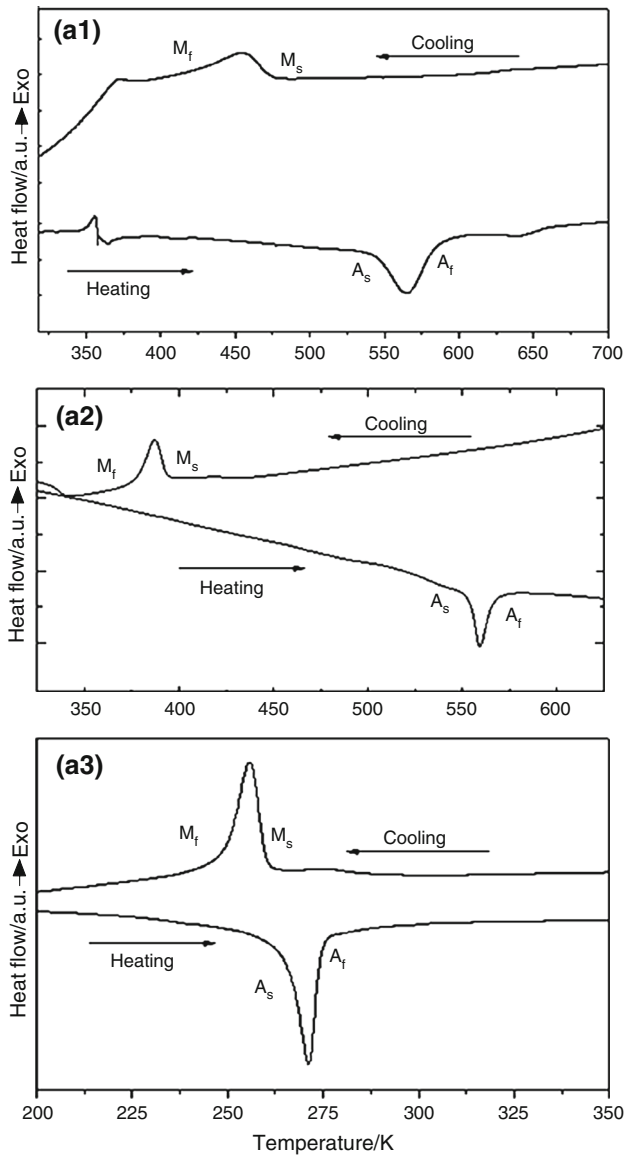

Fig. 3 DSC cyclic scan for the alloys (A1, A2 and A3) at a heating/cooling rate of 10 K min^{-1}. Arrows indicate heating (*up*: austenite to martensite) and cooling (*down*: martensite to austenite)

finish temperatures are M_s, M_f, A_s and A_f, respectively) are determined from the DSC curves. The given hysteresis is due to the increase of the elastic surface energy during the martensite formation. As shown in Table 1, the characteristic transformation temperatures M_s, M_f, A_s and A_f correspond to 475, 410, 540 and 587.5 K, respectively, for A1 ribbons, to 394, 374, 548 and 570 K, respectively, for A2 ribbons and to 274, 265, 286 and 297 K, respectively, for A3 ribbon. In a recent work, from the results of DSC measurements, Khovaylo et al. [22] have determined the characteristic temperatures of martensitic transformation which were found to be $M_s = 281$ K, $A_s = 289$ K for $Ni_{50}Mn_{36}Co_1Sn_{13}$ and $M_s = 303$ K, $A_s = 307$ K for $Ni_{50}Mn_{34}Co_3Sn_{13}$. Furthermore, Zheng et al. [28] have recently reported on higher values ($M_s = 254$ K; $M_f = 235$ K; $A_s = 260$ K and $A_f = 278$ K) for $Ni_{49}Mn_{39}Sn_{12}$ ribbons. Raj Kumar et al. [29] have also described higher transformations temperatures of about 80 K ($M_s = 327$ K; $M_f = 316$ K; $A_s = 328$ K and $A_f = 335$ K) when Sn was substituted by In.

On the other hand, the nucleation of the martensite implies supercooling. The width of the hysteresis, ΔT, is determined as the difference between the temperatures corresponding to the peak positions. The values obtained upon cooling and heating were about 128.75, 175 and 22 K for A1, A2 and A3 ribbons, respectively (Table 1). In addition, the transformation region can be characterized by the martensite transformation temperature T_0 (the temperature at which the Gibbs energies of martensitic and parent phases are related to the M_s and A_f parameters by the equation $T_0 = 1/2(M_s + A_f)$ [30]). The values of T_0 were calculated as about 531.25, 482 and 285.5 K for A1, A2 and A3, respectively.

The DSC curves of the heating and the cooling cycles for the A1 as-spun ribbons exhibit large exothermic and endothermic peaks (Fig. 3a$_1$). For this alloy with low Co content, the coexistence of martensitic and austenitic phases with high levels could influence peaks profiles.

With respect to the change of transition temperatures, it can be interpreted from the following two aspects. Firstly, the Co addition leads to a higher electron concentration (e/a) equal to 8.37. This concentration is calculated using the electron concentration of the outer shells for each chemical component of the investigated alloys as follows:

$$(e/a) = [10x_{Ni} + 7x_{Mn} + 4x_{Sn} + 3x_{In} + 9x_{Co}]/100.$$

At this level, it is assumed that the valence electrons per atom are $10(3d^84s^2)$ for Ni, $7(3d^54s^2)$ for Mn, $4(5s^25p^2)$ for Sn, $9(3d^74s^2)$ for Co and $3(5s^25p^1)$ for In. Secondly, concerning the size effect, the atomic radii are 0.125 nm for Ni, 0.135 nm for Mn, 0.163 nm for Sn, 0.126 nm for Co and 0.162 nm for In. Both factors would make the austenite unstable and therefore lead to the transformation occurring at a higher temperature [31–36].

The entropy and enthalpy changes (ΔS and ΔH, respectively) of the structural transformations are calculated from the baseline calorimetry data [32] as follows:

$$\Delta H = \int_{T_i}^{T_f} \left(\frac{dQ}{dt}\right)\left(\frac{dT}{dt}\right)^{-1} dT$$

$$\Delta S = \int_{T_i}^{T_f} \frac{1}{T}\left(\frac{dQ}{dt}\right)\left(\frac{dT}{dt}\right)^{-1} dT$$

Table 1 Calculated values of enthalpy (ΔH) and thermal entropy (ΔS) changes obtained from cooling (heating) curves

Ribbons	Ms/K	Mf/K	As/K	Af/K	T_0/K	ΔH/J g^{-1}	ΔS/J g^{-1} k^{-1}	*e*/*a*
$Ni_{50}Mn_{37.5}Sn_{7.5}Co_5$	475	410	555	587.5	531.25	51.53 (h)	0.091 (h)	8.375
						51.932 (c)	0.114 (c)	
$Ni_{50}Mn_{42.5}Sn_{7.5}$	394	374	548	570	482	21.206 (h)	0.004 (h)	8.275
						19.484 (c)	0.04 (c)	
$Ni_{50}Mn_{37}Sn_{6.5}In_{6.5}$	274	265	286	297	285.5	6.32 (h)	0.022 (h)	8.045
						6.27 (c)	0.021 (c)	

where T_i and T_f are the temperature limits of integration. The calculated values of enthalpy (ΔH) and thermal entropy (ΔS) changes obtained from cooling (heating) curve are given in Table 1.

The cobalt added instead of Mn in $Ni_{50}Mn_{42.5-x}Sn_{7.5}Co_x$ has a marked effect on martensitic transition temperatures. In $Ni_{50}Mn_{42.5-x}Sn_{7.5}Co_x$, the substitution of Mn by Co significantly affects M_s and M_f, determined from the results of DSC measurements. It is reported that Co doping in $Ni_{50}Mn_3Sn_{7.5}Co_5$ increases the M_s. The substitution of Co by Mn changes the value of *e*/*a*, which can be explained in terms of *e*/*a* (*e*/*a* increase → Ms increase). It has been reported in Ni–Mn–Sn alloys that the characteristic temperatures increase with the increase in the value of the outer electron concentration (*e*/*a*) [37]. This is consistent with the general trend of positive dependence of martensitic transformation temperatures on the *e*/*a* ratio observed in Ni–Mn–*Z* (*Z* = Ga, In, Sn and Sb) and Cu–Al–Z (Z = Mn, Ni) alloys [2, 38–40]. It is to be noted that both the enthalpy and entropy changes increase with the increase in *e*/*a* ratio, caused by Co addition. The influence of *e*/*a* ratio on the entropy change of martensitic transformation has been reported for $Ni_{50}Mn_{50-x}Sn_x$ [32], $Mn_{50}Ni_{50-x}In_x$ [40] and $Ni_{50+x}Mn_{25-x}Ga$ [41] alloys. In these alloy systems, ΔS increases with the increase in transformation temperatures and *e*/*a* ratio, and this is in good agreement with the findings in this study. The tendency of Ms to increase upon the substitution of Co for Mn in Ni–Mn (Sn, Co) is identical to that observed in Ni–Mn (Co, Ga).

Conclusions

In the present paper, we have investigated the structures and martensitic transformation properties of the $Ni_{50}Mn_{37.5}Sn_{7.5}Co_5$ (A1), $Ni_{50}Mn_{42.5}Sn_{7.5}$ (A2) and $Ni_{50}Mn_{37}Sn_{6.5}In_{6.5}$ (A3) ribbons based on the obtained experimental results and some conclusions may be drawn.

1. The results from calorimetric and X-ray diffraction pattern analysis at room temperature confirmed that MT occurred above room temperature for (A1–A2) and below room temperature for (A3). Columnar grains and preferential orientation were obtained from morphological analysis.
2. Martensitic structure is four-layered orthorhombic 4O in sample with Co addition and cubic $L2_1$ in sample with In addition.

Acknowledgements This study was supported by financial funds from the MAT2013-47231-C2-2-P project. The authors would like to express their gratitude to Xavier Fontrodona Gubau for her XRD support. They would also like to thank Professor Layla Mahfoudi from the English Language Unit at the Faculty of Sciences of Sfax (Tunisia) for his constructive language polishing and editing services.

References

1. Manosa Ll, Moya X, Planes A, Krenke T, Acet M, Wassermann EF. Ni-Mn-based magnetic shape memory alloys: magnetic properties and martensitic transition. Mater Sci Eng A. 2008;49:481–2.
2. Krenke T, Moya X, Aksoy S, Acet M, Entel P, Manosa Ll, Planes A, Elermanc Y, Yüceld A, Wassermanna EF. Electronic aspects of the martenistic transition in Ni–Mn based Heusler alloys. J Magn Magn Mater. 2007;310:2788–9.
3. Llamazares JLS, Sanchez T, Santos JD, Pérez MJ, Sanchez ML, Hernando B, et al. Martensitic phase transformation in rapidly solidified $Mn_{50}Ni_{40}In_{10}$ alloy ribbons. Appl Phys Lett. 2008;92:012513.
4. Xuan HC, Xie KX, Wang DH, Han ZD, Zhang CL, Gu BX, Du W. Effect of annealing on the martensitic transformation and magnetocaloric effect in $Ni_{44.1}Mn_{44.2}Sn_{11.7}$ ribbons. Appl Phys Lett. 2008;92:242506.
5. Hernando B, Llamazares JLS, Santos JD, Escoda L, Suñol JJ, Varga R, Baldomir D, Serantes D. Thermal and magnetic field-induced martensite-austenite transition in $Ni_{50.3}Mn_{35.3}Sn_{14.4}$ ribbons. Appl Phys Lett. 2008;92:042504.
6. Santos JD, Sanchez T, Alvarez P, Sanchez ML, Sánchez Llamazares JL, Hernando B, Escoda L, Suñol JJ, Varga R. Microstructure and magnetic properties of $Ni_{50}Mn_{37}Sn_{13}$ Heusler alloy ribbons. J Appl Phys. 2008;103:07B326.
7. Krenke T, Duman E, Acet M, Wassermann EF, Moya X, Mañosa L, Planes A. Inverse magnetocaloric effect in ferromagnetic Ni–Mn–Sn alloys. Nat Mater. 2005;4:450–4.
8. Wang W, Jinke Y, Zhai Q, Luo Zh, Zheng H. Origin of retarded martensitic transformation in Heusler Ni–Mn–Sn melt-spun ribbons. Intermetallics. 2013;42:126–9.
9. Kainuma R, Imano Y, Ito W, Sutou Y, Morito H, Okamoto S, Kitakami O, Oikawa K, Fujita A, Kanomata T, Ishida K. Magnetic-field-induced shape recovery by reverse phase transformation. Nature. 2006;439:957–60.

10. Kainuma R, Imano Y, Ito W, Morito H, Sutou Y, Oikawa K, Fujita A, Ishida K. Magnetic shape memory effect in a Heusler-type $Ni_{43}Co_7Mn_{39}Sn_{11}$ polycrystalline alloy. Appl Phys Lett. 2006;88:192513.
11. Ito K, Ito W, Umetsu RY, Tajima S, Kawaura H, Kainuma R, Ishida K. Metamagnetic shape memory effect in polycrystalline NiCoMnSn alloy fabricated by spark plasma sintering. Scripta Mater. 2009;61:504–7.
12. Sharma VK, Chattopadhyay MK, Kumar R, Ganguli T, Tiwari P, Roy SB. Magnetocaloric effect in Heusler alloys $Ni_{50}Mn_{34}In_{16}$ and $Ni_{50}Mn_{34}Sn_{16}$. J Phys: Condens Matter. 2007;19:496207.
13. Hernando B, Sánchez Llamazares JL, Santos JD, Prida VM, Baldomir D, Serantes D. Magnetocaloric effect in melt spun $Ni_{50.3}Mn_{35.5}Sn_{14.4}$ ribbons. Appl Phys Lett. 2008;92:132507.
14. Recarte V, Pérez-Landazábal JI, Kustov S, Cesari E. Entropy change linked to the magnetic field induced martensitic transformation in a Ni–Mn–In–Co shape memory alloy. J Appl Phys. 2010;107:053501.
15. Khan M, Pathak AK, Paudel MR, Dubenko I, Stadler S, Ali N. Magnetoresistance and field-induced structural transitions in $Ni_{50}Mn_{50-x}Sn_x$ Heusler alloys. J Magn Magn Mater. 2008;320:L21–5.
16. Han ZD, Wang DH, Qian B, Feng JF, Jiang XF, Du YW. Phase transitions, magnetocaloric effect and magnetoresistance in Ni–Co–Mn–Sn ferromagnetic shape memory alloy. Jpn J Appl Phys. 2010;49:010211.
17. Umetsu RY, Ito K, Ito W, Koyama K, Kanomata T, Ishida K, Kainuma R. Kinetic arrest behavior in martensitic transformation of NiCoMnSn metamagnetic shape memory alloy. J Alloys Compds. 2011;509:1389–93.
18. Chen F, Tong YX, Tian B, Zheng YF, Liu Y. Time effect of martensitic transformation in $Ni_{43}Co_7Mn_{41}Sn_9$. Intermetallics. 2010;18:188.
19. Chen F, Tong YX, Tian B, Li L, Zheng YF. Effect of pre-strain on martensitic transformation of $Ni_{43}Mn_{43}Co_7Sn_7$ high-temperature shape memory alloy. Mater Lett. 2010;64:1879–82.
20. Ito W, Xu X, Umetsu RY, Kanomata T, Ishida K, Kainuma R. Concentration dependence of magnetic moment in $Ni_{50-x}Co_xMn_{50-y}Z_y$ (Z = In, Sn) Heusler alloys. Appl Phys Lett. 2010;97:242512.
21. Krenke T, Duman E, Acet M, Moya X, Mañosa L, Planes A. Effect of Co and Fe on the inverse magnetocaloric properties of Ni–Mn–Sn. J Appl Phys. 2007;102:033903.
22. Khovaylo V, Koledov V, Shavrov V, Ohtsuka M, Miki H, Takagi T, Novosa V. Influence of cobalt on phase transitions in $Ni_{50}Mn_{37}Sn_{13}$. Mat Sci Eng A. 2008;481–482:322–5.
23. Srivastava V, Chen X, James RD. Hysteresis and unusual magnetic properties in the singular Heusler alloy $Ni_{45}Co_5Mn_{40}Sn_{10}$. Appl Phys Lett. 2010;97:014101.
24. Umetsu RY, Sheikh A, Ito W, Ouladdiaf B, Ziebeck KRA, Kanomata T, Kainuma R. The effect of Co substitution on the magnetic properties of the Heusler alloy $Ni_{50}Mn_{33}Sn_{17}$. Appl Phys Lett. 2011;98:042507.
25. Liu J, Scheerbaum N, Hinz D, Gutfleisch O. Magnetostructural transformation in Ni–Mn–In–Co ribbons. Appl Phys Lett. 2008;92:162509.
26. Lutterotti L, MAUD CPD Newsletter, IUCr, 2000;24.
27. Petricek V, Dusek M. The crystallographic computing system. Praha: Institute of Physics; 2000.
28. Zheng H, Wu D, Xue S, Frenzel J, Eggeler G, Zhai Q. Martensitic transformation in rapidly solidified Heusler Ni_{49} Mn_{39} Sn_{12} ribbons. Acta Mater. 2011;59:5692–5699.
29. Raj Kumar DM, Sridhara Rao DV, Rama Rao NV, Manivel Raja M, Singh RK, Suresh KG. In-situ phase transformation studies of $Ni_{48}Mn_{39}In_{13}$ melt-spun ribbons. Intermetallics. 2012;25:126–30.
30. Kaufman L, Hullert M. Thermodynamics of martensite transformation. In: Olson GB, Owen WS, editors. Martensite. Cambridge: ASM International; 1992. p. 41.
31. Kainuma R, Umetsu RY. Disorder and strain-induced complexity in functional materials chapter 3: Ni–Mn–X Heusler materials. Mater Sci. 2012;148:49.
32. Krenke T, Acet M, Wassermann EF, Moya X, Manosa L, Planes A. Martensitic transitions and the nature of ferromagnetism in the austenitic and martensitic states of Ni–Mn–Sn alloys. Phys Rev B. 2005;72:014412.
33. Ma SC, Shih CW, Liu J, Yuan JH, Lee SY, Lee YI, Chang HW, Chang WC. Wheel speed-dependent martensitic transformation and magnetocaloric effect in Ni–Co–Mn–Sn ferromagnetic shape memory alloy ribbons. Acta Mater. 2015;90:292–302.
34. Zheng H, Wang W, Jinke Y, Zhai Q, Luo Zh. Martensitic transformation in melt-spun Heusler Ni–Mn–Sn–Co ribbons. J Mater Res. 2014;29:880–6.
35. Bachaga T, Daly R, Suñol JJ, Saurina J, Escoda L, Legarreta LG, Hernando B, Khitouni M. Effects of Co additions on the martensitic transformation and magnetic properties of Ni–Mn–Sn shape memory alloys. J. Supercond Nov Magn. 2015;28:3087–92.
36. Zhang Y, Zhang L, Zheng Q, Zheng X, Ming L, Juan D, Yan A. Enhanced magnetic refrigeration properties in Mn-rich Ni–Mn–Sn ribbons by optimal annealing. Sci Rep. 2015;5:11010.
37. Coll R, Escoda L, Saurina J, Sanchez-Llamazares JL, Hernaudo B, Sunol JJ. Martensitic transformation in Mn–Ni–Sn Heusler alloys. J Therm Anal Calorim. 2010;99:905–9.
38. Safaa NS, Hamzah E, Abubakar T, Zamri M, Tanemura M. Influence of Ti additions on the martensitic phase transformation and mechanical properties of Cu–Al–Ni shape memory alloys. J Therm Anal Calorim. 2014;118:111–22.
39. Adorno AT, Silva RAG. Effect of Ag additions on the reverse martensitic transformation in the Cu-10 mass% al alloy. J Therm Anal Calorim. 2006;83:241–6.
40. Bachaga T, Daly R, Escoda L, Suñol JJ, Khitouni M. Influence of chemical composition on martensitic transformation of MnNiIn shape memory alloys. J Therm Anal Calorim. 2015;122:167–73.
41. Khovailo VV, Oikawa K, Abe T, Tagaki T. Entropy change at the martensitic transformation in ferromagnetic shape memory alloys $Ni_{2-x}Mn_{1-x}Ga$. J Appl Phys. 2003;93:8483–5.